Relationships between SSTs, air temperature, and coastal fog using field data and satellite remote sensing

Isabella Fatland[1,2], Jessica Lundquist[1,3]

REU-Blinks Program 2025
Summer 2025

[1] Friday Harbor Laboratories, University of Washington, Friday Harbor, WA 98250
[2] Department of Earth and Atmospheric Sciences, Cornell University, Ithaca, NY 14853
[3]Department of Civil and Environmental Engineering, University of Washington, Seattle, WA 98195

Contact Information:
Isabella Fatland
icf25@cornell.edu

Keywords: sea surface temperature, coastal fog, marine-atmosphere interactions

Abstract

Understanding how sea surface temperature (SST), air temperature, and coastal fog interact is increasingly important for studying climate refugia in coastal environments, increasingly so as the climate warms and coastal zones are exposed to more extreme conditions during the summer. Using Landsat imagery, in situ air temperature and relative humidity (TRH) data, time-lapse camera imagery, and Conductivity Temperature Depth sensor (CTD) profiles, we studied spatial and temporal variability in these components of ocean-atmosphere interaction around San Juan Island, WA. SSTs derived from Landsat images from summer 2021-2024 showed consistent temperature differences between warmer water at the north end and colder water at the south end of the island. Air temperature differences between sites typically followed SST patterns, but correlations varied with local weather patterns. Time-lapse camera imagery and TRH data showed foggy days to be cooler and more humid than clear days. CTD casts showed strong short-term stratification during rising tides and indicated upwelling in certain regions, suggesting that mechanical mixing may influence SST variability. These results refine our understanding of how local ocean-atmosphere interactions can influence temperature and fog formation and can help identify coastal climate refugia.

1. Introduction

The Salish Sea contains a lot of diversity, both in local organisms and in the types of environments that they inhabit. Because of this, it is a model location to study microclimates. Estuarine circulation, regional trends, coastal fog and cloud cover, and many other features of coastal environments are complex and difficult to predict patterns in. Research on microclimates is increasingly important as climate change continues to impact ecosystems, and these characteristics of the marine-atmosphere boundary layer (MABL), in variable and unpredictable ways.

This summer, we sought to better understand how and why features such as sea surface temperature (SST), coastal fog frequency, and air temperature vary by location around San Juan Island, using a combination of Landsat data and field data measurements to better predict which areas might serve as more successful climate refugia in the future.

Our scope included the following questions:

- How do air temperature variations around San Juan Island correspond to SST differences? (section **3.2)**

- How do SSTs vary at different coastal locations around San Juan Island? (section **3.3**)

- How does fog frequency and duration compare with SSTs and Air Temperature (AT)? (section **3.4**)

- How does the water profile in the San Juan Channel vary in stratification, temperature, and salinity at different locations? (section **3.5**)

2. Background

2.1 Regional Information

The Salish Sea refers to the region of the Pacific Northwest including the Strait of Juan de Fuca, the Strait of Georgia, and Puget Sound, and forms a large estuarine system. The San Juan Islands are situated in the middle of that system. The Strait of Juan de Fuca brings in cold, salty water from the Pacific Ocean (during a rising tide, or flood tide), while the Strait of Georgia brings down a mix of salty and warmer freshwater (during an ebb tide), mostly from the Fraser River (MacCready et al., 2020). Freshwater from the Fraser River stays in the top 10 meters of the water column as it is brought southward towards the San Juan Islands, where tidal mixing is very strong, and the water column can become completely mixed from top to bottom in some places (Pawlowicz et al., 2019). As a result, during the summer there can be dramatic differences in Sea Surface Temperatures (SSTs) and salinity across relatively small distances within this system.

The ocean surface acts as a bridge between ocean waters and the Marine-Atmosphere Boundary Layer (MABL). Many features of the MABL, such as air stability and temperature, winds, and coastal fog cover, respond dynamically to SST variations, and a lot remains uncertain about how these patterns arise and function. As SSTs increase with climate change, understanding how the MABL interacts with the ocean continues to be an important area of research (Borgnino et al., 2025).

2.2 Air Temperature

2.2.1 Air Temperature Influence by SSTs

Air Temperature can be strongly influenced by SSTs, especially in coastal areas. The sea breeze is one phenomenon that connects air temperature with SSTs. During the day, the sun warms the ground and ocean. However, the air over the ground heats faster than the air over the ocean, which creates a pressure gradient that allows cooler, marine air to come inland and cool the air over coastal land (Miller et al., 2003). These effects vary by season; in the northeast Pacific, SST correlates the most with minimum surface air temperature during the warm season, and maximum air temperature correlates the most in March (Mass et al., 2022).

2.2.2 Temperature Patterns on San Juan Island

On San Juan Island, inland and coastal site temperatures vary year-round. In winter months, inland, high-elevation sites such as Mt. Dallas become much colder than coastal sites due to elevation differences. Coastal sites around the island during this time-period remain similar to each other in air temperature. In the summer, however, inland sites become much warmer than coastal ones. Furthermore, the air temperature at different coastal locations can be extremely different on some days, with locations on the North end of the island becoming much warmer than ones on the South end, for example Cattle Point. (Nguyen et al., 2023).

2.3 Coastal Fog

2.3.1 Fog Formation

Marine fog forms as a result of many different physical processes, including the microphysics of fog formation, the influence of large-scale circulations, precipitation and clouds, radiation, air-sea interaction and resulting turbulence, and advection (Koračin et

al., 2013). For the scope of our project, we focused on the central concept that marine fog forms when warm, near-saturated air moves over relatively colder water.

2.3.2 Fog Influence and Response to Climate Change

Coastal fog is a common feature along the West Coast of North America and impacts coastal regions in many ways: it protects ecosystems and provides an important source of moisture, impacts public health and many industries, and can contribute to aviation-related and other accidents (Dye et al., 2024). Fog and low cloud cover (FLCC) are an important feature of the Western coastline and have been studied and modeled extensively in California (e.g., O'Brien et al., 2013; Rastogi et al., 2016; Torregrosa et al., 2015). However, FLCC in the Pacific Northwest area remains understudied and difficult to predict and model. Additionally, the complex geography of the Salish Sea, our region of interest, makes it more difficult to study with lower-resolution satellite remote sensing methods previously used to study California FLCC, like GOES (Geostationary Operational Environmental Satellite) and MODIS (Moderate Resolution Imaging Spectroradiometer).

Tidal cycles are considered independent of the changing climate but still affect how intertidal ecosystems respond to increasingly harmful local conditions, such as direct exposure to solar radiation (Mislan et al., 2009). During the summer in the Northeast Pacific, low tides often occur at midday, exposing intertidal organisms to hotter conditions. In comparison, lower-latitude locations in California experience fewer hours of low-tide midday exposure (Helmuth et al., 2002). We believe that frequent marine and coastal fog can act as a cover for exposed intertidal organisms, blanketing them from direct exposure to these harmful conditions. Johnstone & Dawson (2010) showed that

summer marine fog frequencies have decreased by 33% since the early 20th century along the California coast. Decreasing marine fog, increasing air temperatures, and consistently high exposure of intertidal zones in summer months make the Salish Sea a very important zone to study.

2.4 Water Profile

In addition to effects on the MABL, changing SSTs affect processes beneath the surface. Studying microzooplankton biomass changes in southern California, Roemmich and McGowan (1995) explain that, from 1951 to 1995, the surface layer warmed by more than 1.5°C in some locations, leading to a larger temperature difference across the thermocline. More stratification in the water column leads to less wind-driven upwelling of the thermocline, which in turn provides fewer nutrients from deeper waters. Khangaonkar et al. (2019) simulated that between 2000 and 2095, average Salish Sea temperature will increase by +1.51°C, dissolved oxygen will decrease by -0.77mg/L, and acidification by -0.18. The study stressed the growing urgency of a need to understand coastal water and estuarine resilience to climatic changes. Another study on fjord systems along the Salish Sea found in data from 1951 to 2020 that deep water temperature in four inlets increased by 1.2 - 1.3 degrees Celsius over that time period, which is up to twice the global average for open ocean waters at the same depths (Jackson et al., 2021).

In summer months, the water column in some coastal areas becomes more stratified due to solar heating. Specific to the Salish Sea and other estuaries, this stratification can become even more intense due to contributions of warm freshwater. Studies on how increasing surface temperature and water column stratification affect coastal organisms further show the importance of studying water profiles in coastal

zones. Bashevkin et al. (2016) found that lower salinities decreased the posterolateral arm length and swimming ability of *Pisaster ochraceus* larvae, and that continued intensification of influence from the Fraser River could affect sea star populations in the future. In a study on coastal oyster populations in Omura Bay, Japan, artificial upwelling was found to counteract decreased water quality conditions caused by increased summer stratification of the water column (Mizuta et al., 2014).

2.5 Instrument Information and Validation

2.5.1 Live Ocean

The Live Ocean model utilizes the Regional Ocean Modeling System and includes Oregon, Washington, and Vancouver Island coastal waters. Its grid has lines of constant latitude and longitude with 500-meter spacing, and its vertical coordinate system has 30 layers spaced between the bottom and surface of the water. Spacing between layers is smaller near the top and bottom of the water layer, with larger spacing in the middle of the water column. Intertidal zones and zones with depths of less than 4m are not included in the model. Extensive comparisons of three years of past predictions with observations have been made. These comparisons tell us that the model fields for salinity and temperature are reasonably similar to observations, and that we can use this model to explore estuarine exchange flow (MacCready et al., 2021).

2.5.2 Landsat

The Landsat program is managed by NASA and the U.S. Geological Survey (USGS). Currently, the Landsat 8 and 9 satellites orbit Earth at an altitude of 705 km, completing an orbit every 99 minutes and crossing each point on Earth every 16 days.

Their paths are offset so that any Landsat scene area is imaged every 8 days from 2022 onwards. The Operational Land Imager (OLI) has spectral bands with 30-meter resolution, while the Thermal Infrared Sensor (TIRS) captures data with 100-meter resolution, which is then re-sampled to 30 meters (Earth Resources Observation and Science Center, 2017).

Previous studies have examined the accuracy of Landsat for high-resolution SST monitoring in coastal environments. Specific to the Northeast Pacific, Wachmann et al. (2024) compared in situ observations from 1984 to 2021 at four different locations with varying coastal conditions throughout the Salish Sea to Landsat SSTs. It was reported that sensor-specific calibration uncertainty can be minimized by excluding low-temperature images and ensuring that there are no clouds within close proximity of sites of interest. They claimed that Landsat 8 has proven to be a reliable source for SSTs for spring and summer and can be a helpful tool for monitoring temperature conditions off the west coast of Canada. Vanhellemont et al. (2022) used in situ measurements of median sea surface temperature from surfing sessions in Ireland and California with various devices and came to the main conclusion that mixed pixel effects from the warmer land surface can become an issue when using Landsat data close to an ocean-land boundary. Jang and Park (2019) used in situ temperature measurements from buoys on the Korean coast to study Landsat SSTs and reported that errors were related to atmospheric water vapor, wind speed, and satellite zenith angle.

While Landsat SSTs have been reported to contain small levels of error, due to many atmospheric effects and especially in areas in close proximity to coasts, literature

agrees that Landsat's high spatial resolution is a valuable tool for researchers to understand trends of upwelling and temperature differences in coastal regions.

2.5.3 Sontek Castaway CTD

A Sontek Castaway CTD was used to take measurements throughout the water column. For this project, the processed data from the CTD was used to look at ocean profiles, rather than the raw data. While we have not yet found a specific algorithm available that explains how the processed data values are derived, we believe that water property values such as temperature are calculated as a weighted average between the two values at each pressure recording, one on the way down and one on the way up.

3. Methods

3.1 Resources

3.1.1 Field Equipment

Temperature and relative humidity (TRH) HOBOware sensors are set up at locations around the island, including the FHL NOAA station, Cattle Point, Mount Dallas, and other inland and coastal sites (Figure 1). These sensors have been used since August 2021 to collect air temperature and relative humidity data every thirty minutes running from mid-June or mid-July onwards, year-round. For this study in particular, the following locations were used for each summer:

2021 and 2022: FHL and Cattle Point

2023 and 2024: Near Reuben Tarte County Park (or North Island (NI)), FHL, and Cattle Point.

Figure 1: A map of San Juan Island, marked with key field locations.

Figure 2: A close-up map of the FHL campus and dock, with key locations marked.

Similarly, time lapse cameras are set up at these sites around the island and capture images of the area every 30 minutes during the daytime, typically 7:00am to 9:00pm. The cameras are pointed out over the water and monitor cloud cover throughout the summer and fall. Additional footage from cameras at Mt. Dallas, False Bay, and Griffin Bay is also used to monitor cloud cover and frequency.

Figure 3: Field equipment – WingScape time lapse cameras and a HOBOware TRH sensor.

Figure 4: Timelapse images taken at Cattle Point and FHL on 2022-09-30, showing the dissipation of fog over the course of a morning.

A Sontek CastAway Conductivity, Temperature, and Depth sensor (CTD) was used to collect profiles of the water column at the following locations:

1. the FHL dock

2. along the San Juan Channel
3. At 3 locations around the island in shallow intertidal water: Reuben Tarte County Park, Cattle Point, and near the San Juan Golf Club.

A 25-foot research vessel, the Flying Bosun, was used to facilitate CTD experiments. An infrared temperature sensor was also used to gather in situ surface temperature at sites of CTD deployment.

3.1.2 Live Ocean Model

Past Live Ocean model data for Sea Surface Temperatures (SSTs) were compared with Landsat SST readings to evaluate model skill. Live Ocean model forecasts for Summer 2025 were used to form hypotheses about when fog might form during the summer, and when and where there might be larger differences in SSTs.

3.1.3 Gathering, Filtering, and Processing Landsat Scenes

We used Python to download Collection 2 Level-2 Landsat scenes from Microsoft's Planetary Computer, using code developed by Eli Schwat and Jessica Lundquist (https://github.com/elischwat/summerfog). We searched for and downloaded images that included the San Juan Islands taken between 06/30 and 09/30 for 2021 through 2024. Then, for each downloaded image, using the proper scaling and offset numbers, we calculated the temperature for each pixel from the long wave infrared band (LWIR11). We then plotted each scene in two ways using Pyplot:

1. With the calculated temperature pixel values, to check for image quality and obvious cloud cover, since most clouds show up as much colder than the ocean or land.

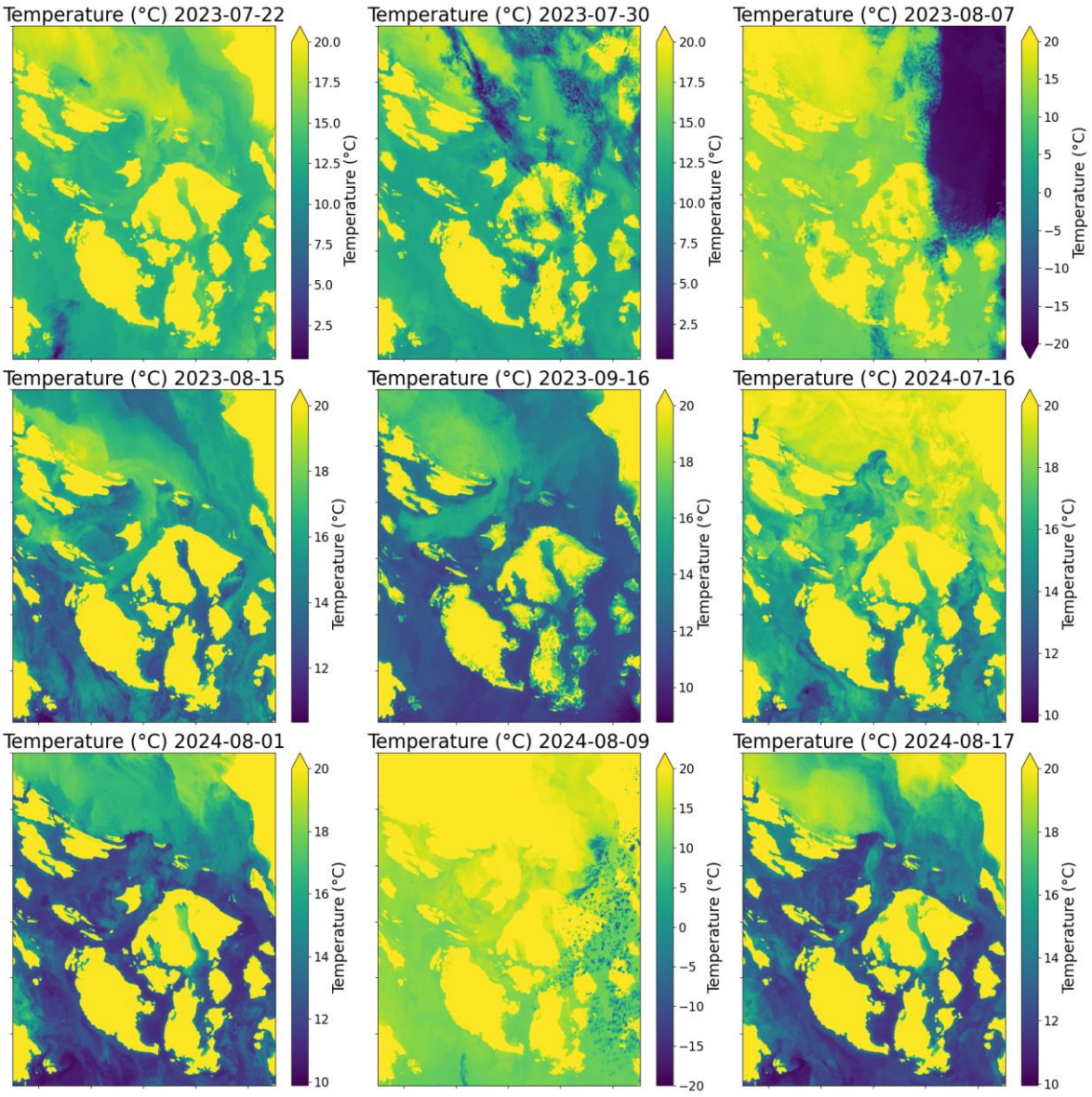

Figure 5: Nine Landsat scenes plotted with Temperature (°C), with dates. The maximum temperature on the color bar has been capped at 20°C, while minimum values differ from scene to scene to show the different cloud temperatures recorded. The color bar on the right shows the temperature range of each image; bluer indicates a lower temperature, yellow indicates warmer.

2. We used NIR08, SWIR16, and Blue bands to make less-cold clouds stand out more against the land and ocean, to ensure that we were not evaluating SST against the temperature of a low-lying cloud.

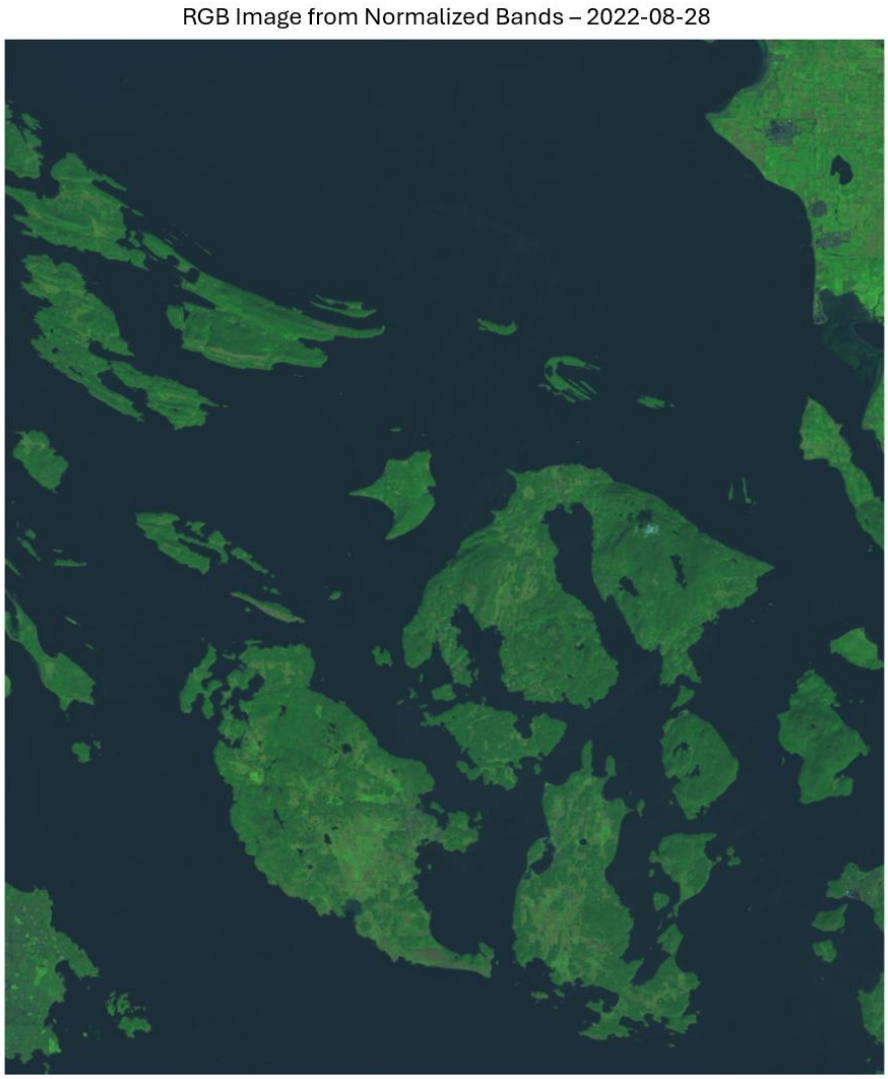

Figure 6: Landsat scene from 2022-08-28, formed by combining NIR, SWIR, and Blue bands. No clear clouds are visible over water from this image, only a small cloud over the northeast side of Orcas Island.

These plots allowed us to determine which images were useful for extracting temperature data from pixels (no clouds over our areas of interest) and which images were not useful (widespread or difficult-to-identify cloud cover).

For some scenes, it was more difficult to determine if some images contained low, warmer clouds. For images that we had timelapse camera footage for, we checked for visible clouds in those frames. Additionally, we replotted the images by limiting the maximum and minimum temperature values to be closer together, to better distinguish between the cooler regions. This allowed us to see image-quality issues and more discreet clouds.

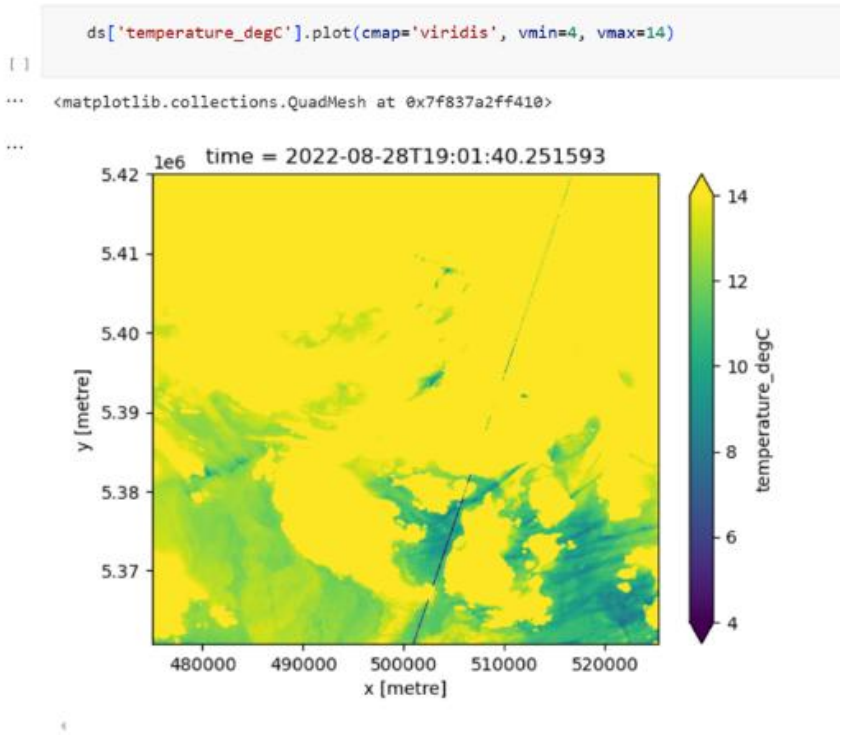

Figure 7: Temperature map of the San Juan Islands 12:00 on 2022-08-28, with an upper temperature bound of 14 and a lower bound of 4, showing wispy clouds in bottom right quadrant. A diagonal line is visible across the photo, cutting across Cattle Point.

We also used the visible Red, Green, and Blue bands and stretched them, which revealed more cloud-like 'texture' that was harder to see with other band combinations.

```
# Normalize R, G, B bands
ds["red_normalized"] = ds["red"] / np.max(ds["red"])
ds["blue_normalized"] = ds["blue"] / np.max(ds["blue"])
ds["green_normalized"] = ds["green"] / np.max(ds["green"])

# Create RGB image
rgb_image = np.stack([
    ds['red_normalized'].values,
    ds['green_normalized'].values,
    ds['blue_normalized'].values
], axis=-1)
```

```
# Trim out highest reflectance values
for i in range(3):
    P = np.percentile(rgb_image[:, :, i], [1, 85])
    rgb_image[:, :, i] = (rgb_image[:, :, i] - P[0]) / np.diff(P)
    rgb_image[:, :, i] = np.clip(rgb_image[:, :, i], 0, 1)
```

```
fig, axes = plt.subplots(1, 2, figsize=(15,7.5))
axes[0].imshow(rgb_image)
axes[1].imshow(rgb_image ** 0.5)
plt.show()
```

Figure 8: Code borrowed from Eli Schwat's GitHub repository - https://github.com/elischwat/summerfog – to plot RGB Landsat scenes.

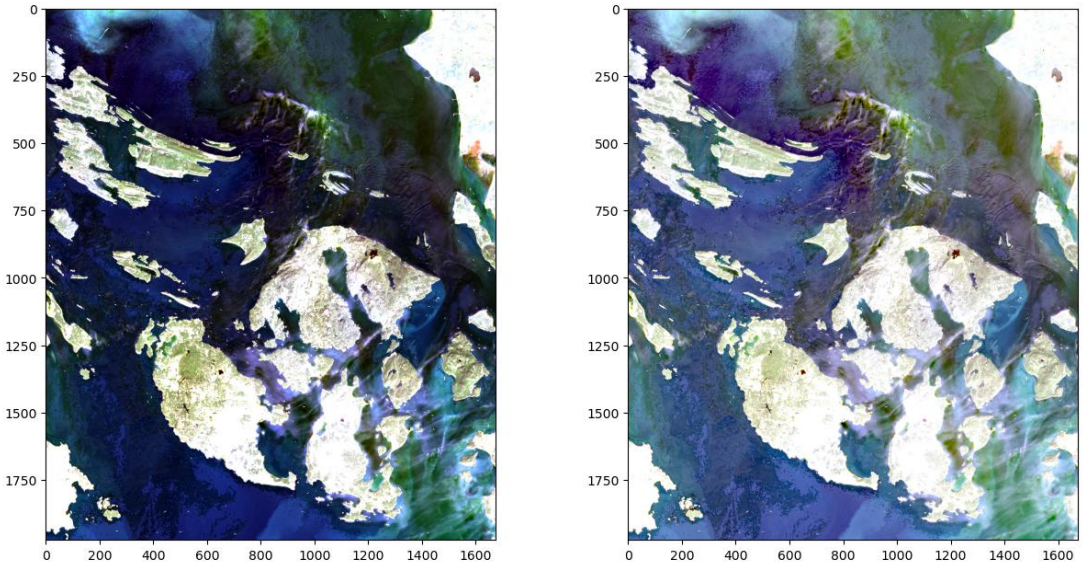

Figure 9: Left: regular RGB image. Right: The same image, but with each pixel value raised to the power of 0.5. This increases contrast between darker regions, making variations over the dark ocean more visible.

All these visual tests were combined to identify which Landsat scenes could be used reliably for SST analysis.

3.2 Comparing Air Temperature Differences to SST Differences

3.2.1 Collecting Landsat SSTs

For each coastal TRH sensor listed in section **2.1.1**, we found coordinates on the nearby section of water, far out enough for the satellite imagery to not be contaminated by warmer pixels on the shore. The heating effect of the shore on the nearby ocean water is not substantial, but Landsat surface temperature pixels near large temperature contrasts can be inaccurate. The coordinates chosen are listed here:

North Island: (-123.090802, 48.608886)

FHL: (-123.000844, 48.545540)

Cattle Point: (-122.952554, 48.465113)

For each Landsat image collected that passed our quality control (described above), we did the following at each of the three locations:

1. Converted Latitude-Longitude coordinates from the map to UTM coordinates for each location of interest (Cattle Point, FHL).
2. Drew a small circle over a collection of pixels centered on those water coordinates, 300 meters in radius
3. Extracted the SST values for each circle of pixels, averaged them, and recorded that mean value.

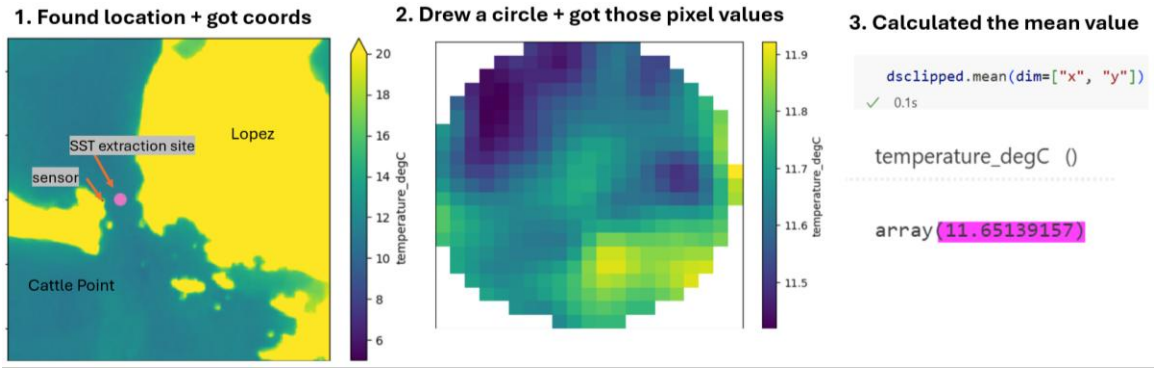

Figure 10: Example images of 3 steps to extract SSTs, using the Landsat scene from 2024-08-01.

3.2.2 Air Temperature and Sea Surface Temperature Differences

We compared Landsat data used from summer 2021 – 2024 with Cattle Point air temperature data from the HOBOware TRH records. For the FHL location, official weather station data was used in place of the TRH data we collected. This was because

our field sensor was being hit by sunlight and warmed in the middle of the day, giving us inaccurate air temperature data. For each day with quality-controlled Landsat SSTs, we calculated the difference in air temperature at FHL and Cattle Point at 12:00, 13:00, and 14:00. Differences between FHL and Cattle Point SSTs from section **3.2.1** were calculated as well.

For the summers of 2023 and 2024, using air temperature data from NI and SSTs from water near there, the process was repeated to compare temperatures between the North end of the island, FHL, and Cattle Point, as three transects from the north to south ends of the island. Across the separate locations, we looked at the varying air temperatures and SSTs to see if larger differences in SST correlated with larger differences in air temperature.

3.2.3 Dew Point Temperature and Sea Surface Temperature Differences

Our HOBOware TRH sensors supplied calculated Dew Point Temperature (DPT), but we had incomplete records of it for different years. Additionally, since the TRH data from the FHL NOAA station didn't have DPT, we decided to use the same calculations for all TRH locations to be consistent.

DPT was calculated using equations detailed in Feld et al. 2013:

$$E_{sat} = 610.94(\text{Pa})\exp\left(\frac{17.625T}{243.04°\text{C} + T}\right) \quad \text{(A2)}$$

[60] In hydrological applications, we are often concerned with the ratio of the amount of water in the atmosphere over the amount of water that the atmosphere can hold. This ratio is called the relative humidity (RH, %) and can be defined as

$$RH = 100\frac{E_a}{E_{sat}} \quad \text{(A3)}$$

[61] The dew point temperature (TD, °C) is the temperature at which the air will be saturated for a given amount of water vapor. This can be calculated from the actual amount of water vapor in the air (E_a) as determined from relative humidity and the Magnus formulation for vapor pressure at the dew point temperature:

$$TD = \frac{243.04°\text{C}\ln(E_a/610.94)}{17.625 - \ln(E_a/610.94)} \quad \text{(A4)}$$

(Feld et al., 2013).

Figure 11: A screencap of Feld et al.'s paper, with the relevant conversion equations to calculate Dew Point Temperature.

We then calculated differences between sites and compared them to SST differences, using the same days, locations, and intervals as with air temperature differences.

3.3 SST Variations by Site

After filtering all available Landsat scenes, ones with either:

1. no visible clouds

or

2. minimal clouds, only over land

were combined into a single scene to look for water temperature trends. 8 scenes from 2021 – 2024 summers fit these criteria: 2021-09-02, 2022-07-11, 2022-07-27, 2022-09-21, 2023-08-15, 2024-07-16, 2024-08-01, and 2024-08-17.

This was accomplished by using Python xArray functionality to stack the scenes together and get the mean value of each pixel. When plotting the image, pixel values were capped to a maximum of 20°C to flatten land temperatures and better see differences in SSTs. This was done by setting the maximum value on the color bar to 20°C and did not change any of the calculated pixel values.

```
# getting the mean Landsat scene for temperature
dsa = [ds['temperature_degC'] for ds in dss]
temp_stack = xr.concat(dsa, dim='dataset')
mean_temp = temp_stack.mean(dim='dataset')

mean_temp.plot(vmax = 20)
plt.title('mean temp')
plt.show()
```

Figure 12: A sample of code showing the process by which the mean Landsat image was compiled.

This scene was used to look at overall spatial patterns in SSTs and compared against a bathymetry map/nautical chart of the area.

3.4 Fog Frequency and Duration Compared to Air Temperature Data

For time lapse footage that we had from summers 2021-2024, we went through each day and categorized them into one of three categories:

1. Cloudy – significant clouds at any point of the day. This includes rainy days, overcast mornings that turned into sunny days in the afternoon, and foggy days that were also cloudy.
2. Clear – sunny and blue skies all day, with minimal or no clouds.
3. Fog and then Clear – days that started with low fogbanks and clear skies afterwards.

To simplify, we disregarded cloudy days. We analyzed days that were clear all day (clear days, CDs) and days that had fog in the morning and then became clear (foggy days, FDs).

With our record of CDs and FDs, we utilized our TRH data to plot various time series of each day. CDs were plotted with red, and FDs were plotted with blue.

Mean Air Temperature (AT), Relative Humidity (RH), and Dew Point Temperatures (DPT) (calculated in section **3.2.3)** were plotted to develop an understanding of how those air properties might differ on days with and without fog.

3.5 Water Profile and CTD Experiments

3.5.1 CTD casts at the FHL dock

On 9 July 2025, CTD casts were collected off the FHL dock every hour from 9:30am to 7:30pm using an approximately 10-meter rope, to look at how a small-scale water profile changes over the course of a rising tide. The casts were done on the interior of the dock, right next to the NOAA water temperature sensor (Figure 2).

3.5.2 CTD casts in the San Juan Channel

On 20 July 2025, we went out on the research vessel Flying Bosun to do CTD casts in the San Juan channel from 8am to 3pm. Casts were performed using a downrigger to lower the CTD into the water. The protocol for each cast went as follows:

1. Use IR sensor and record SST at location.
2. Start CTD cast and lower it until submerged in water.
3. Mark location on Flying Bosun navigation system.

4. Wait ten seconds for CTD to record surface temperature, then begin reeling out the downrigger at a consistent pace.

5. Once having reeled out 86 rotations worth of cable, reel the CTD back up at a consistent pace - this corresponded to about 40 meters of depth.

The survey was conducted during a period of flood tides, which induced northward-moving currents. To account for drifting due to Northward-moving currents, we relocated back to the mark on the vessel navigation system. Then, we repeated the same process at the same location, so that at every location we had two similar casts.

The day was divided into four main sections (Figure 13):

1. Going along the South end of Shaw Island (8:30 – 9:30am, early rising tide)

2. Going down the San Juan channel to Cattle Point (9:30 – 11:45am, early rising tide)

3. Going into the South end of Griffin Bay (11:45am – 12:45pm, middle of rising tide)

4. In the afternoon, revisiting locations to the South of Shaw Island (3:30pm, middle of rising tide)

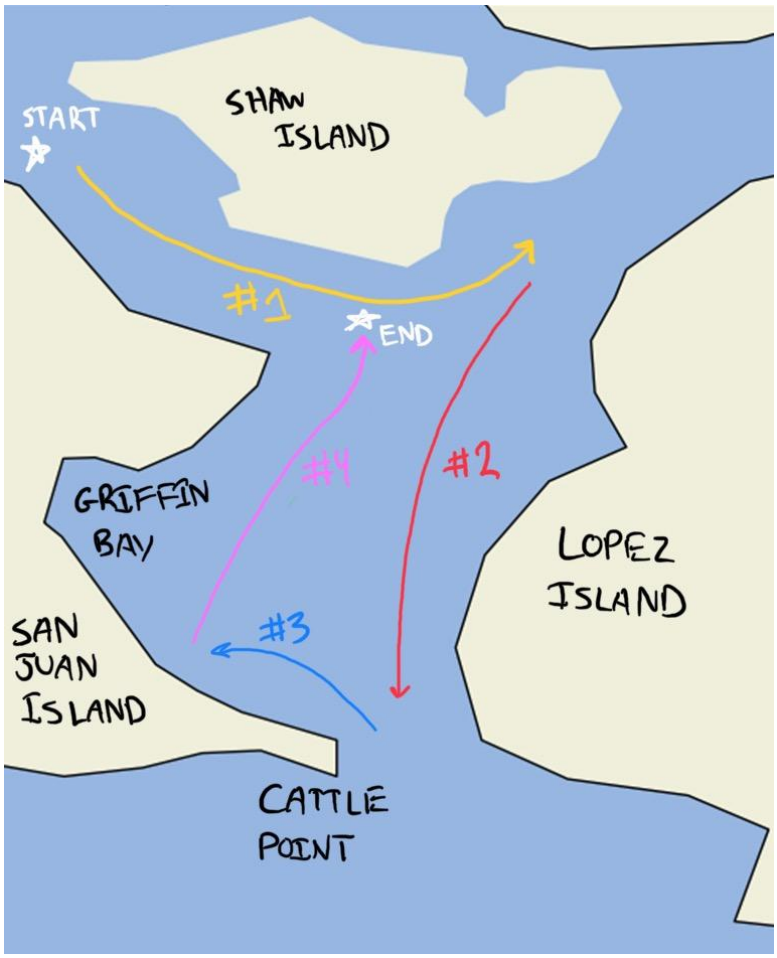

Figure 13: A map showing the route of the Flying Bosun on 20 July 2025. We started in the top left corner, near FHL. Arrows numbered 1 through 4 match the sections previously described

We then processed the CTD data and plotted two water properties - temperature and salinity – against depth. This allowed us to develop a further qualitative understanding of how those properties varied with time and space.

4. Results

4.1 AT and SST Differences

4.1.1 All SSTs

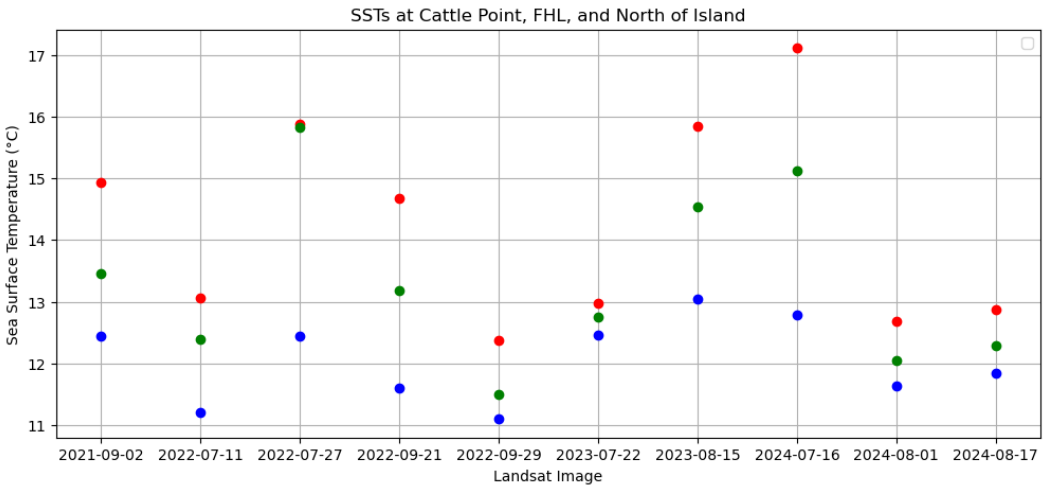

Figure 14: SSTs at Cattle Point (blue), FHL (green) and NI (red) across 10 Landsat images.

For the ten Landsat images that we collected SSTs from, we saw that the SST at the North end of the island (NI) was consistently warmer than the SST collected from near FHL and Cattle Point. We also can see that the FHL SST is consistently warmer than the Cattle Point SST. This order is present in all ten days, but the differences in temperature vary in amplitude and uniformity. On most days, the three data points are somewhat equally spaced apart, like 2021-09-02 and 2022-09-21, where differences in SSTs are around 1-1.5°C. On other days, like 2023-07-22, the three points still have uniform spacing, but differences in value of less than 0.3°C. On 2022-07-27, the SSTs at

NI and FHL are almost the same, almost 16°C, while Cattle Point is much colder, at around 12.5°C.

4.1.2 Air Temperatures

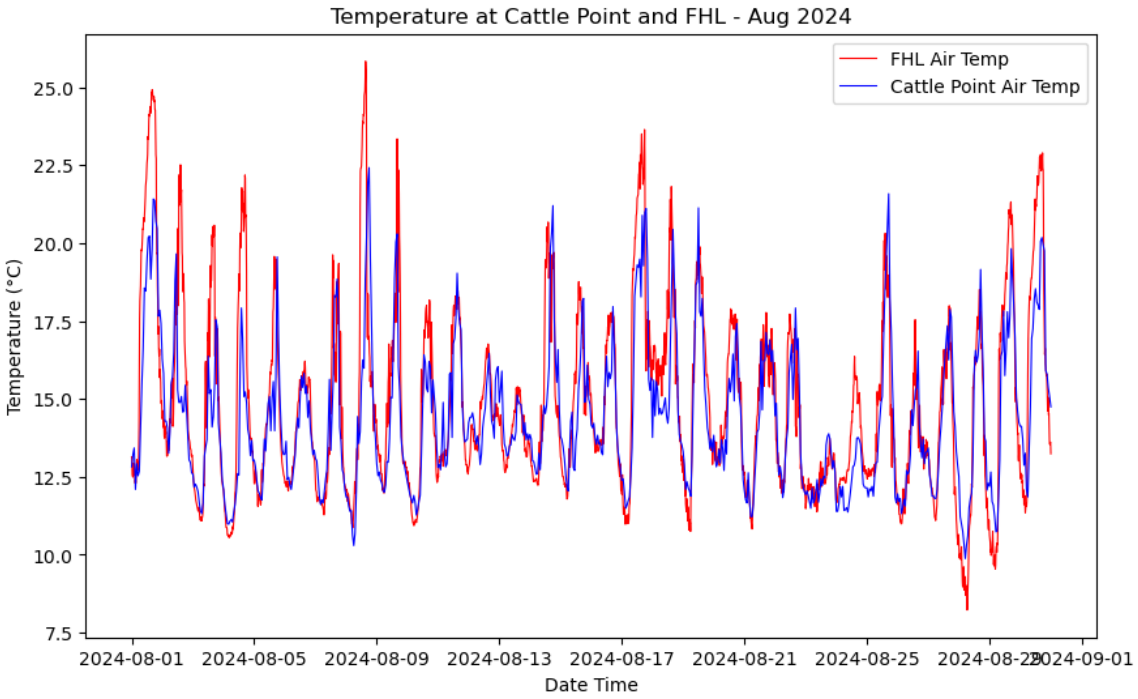

Figure 15: An example timeseries showing air temperature at FHL and Cattle Point, from 2024-08-01 – 2024-09-01.

Qualitatively, from time series showing air temperature records from different island locations, we can see that FHL is sometimes much hotter in the middle of the day than Cattle Point. At other times, they match pretty well throughout the day in temperature, and rarely, Cattle Point is warmer than FHL.

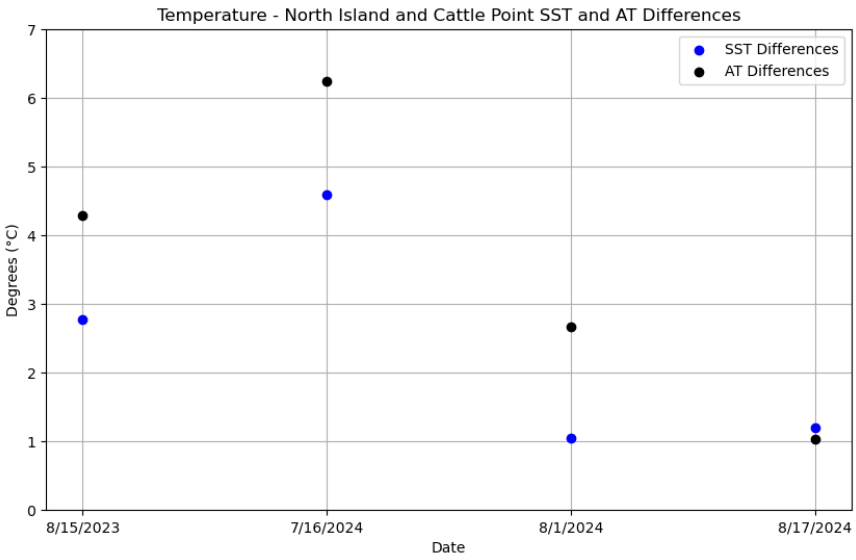

Figure 16: Air Temperature and SST Differences between NI and Cattle Point on Four Landsat Days – 2023-08-15, 2024-07-16, 2024-08-01, and 2024-08-17. Note that the time of day for all of these is near local noon.

As the TRH sensor at the NI location has only been deployed for two summers, we were working with a more limited number of Landsat scenes that we could use to compare air temperature records against. With the comparison of four temperatures, we can see that positive SST differences and positive AT differences coincide, but we need more data to say more about a strong relationship.

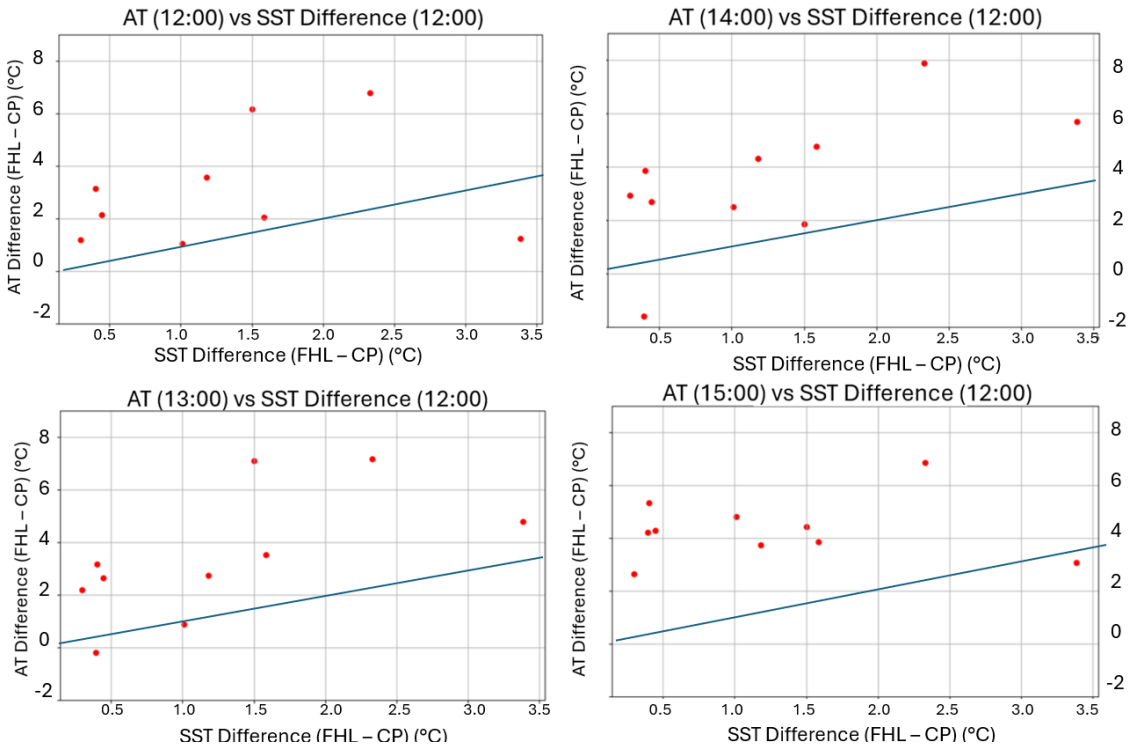

Figure 17: SST difference (FHL – CP) at 12:00 versus AT difference (FHL – CP) at 12:00 (top left), 13:00 (bottom left), 14:00 (top right), and 15:00 (bottom right). Each orange on a plot represents a different Landsat day. A 1:1 blue is included to highlight that AT differences are much larger than SST differences.

Comparing FHL and Cattle Point across ten Landsat images, for four hours, we can again see that most SST difference and AT difference values are positive, but again there is no clear relationship. As time goes on, we can expect that SSTs will stay more consistent than ATs, which change more rapidly. Looking at afternoon-hour AT differences, like 15:00, compared to 12:00 SST differences, we can see that the range of air temperature difference values becomes slightly smaller.

4.2 SST Patterns by Coastal Location Using Landsat

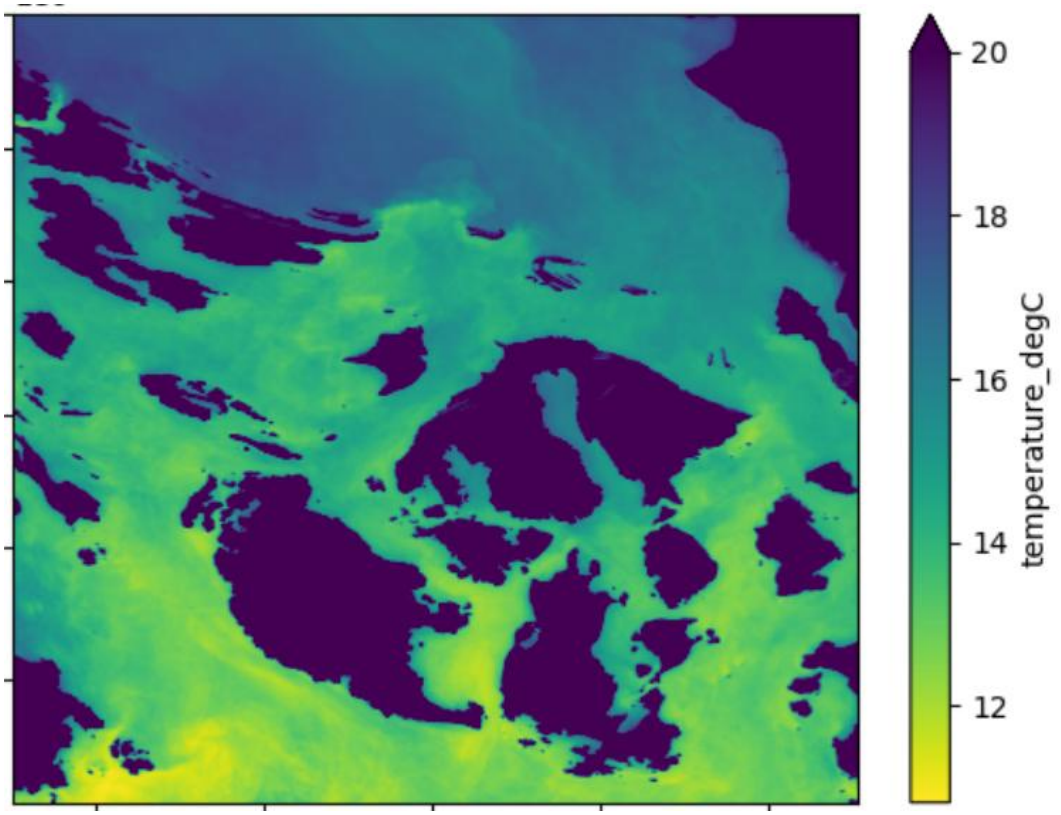

Figure 18: A single scene formed from 8 Landsat scenes (2021-09-02, 2022-07-11, 2022-07-27, 2022-09-21, 2023-08-15, 2024-07-16, 2024-08-01, and 2024-08-17) with no clouds found, where each pixel represents the mean temperature from those 8 scenes. The scale has been capped at 20°C to better show differences in SST, with a minimum of 11°C. The color bar has been inverted so that yellow represents the coldest temperature and dark blue represents the warmest to better highlight contrasts.

In this stacked Landsat image, we can see differences in water temperature between the north and south ends of the island. Furthermore, locally at the south end, we can see patches of distinctly cooler water. A line of cold water runs parallel to the southwest coast of San Juan Island. The south part of the San Juan Channel is notably colder than the water between San Juan Island and Shaw Island. Griffin Bay is warmer than that part of

the San Juan Channel. There is also a patch of colder water to the south of Roche Harbor on the West side of the island.

4.3 Fog Frequency and Duration Compared to Air Temperatures

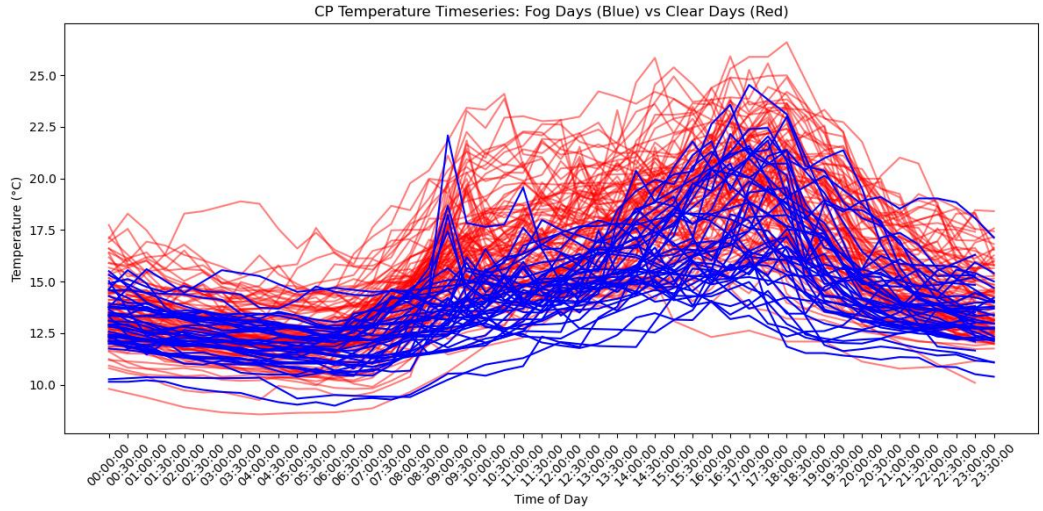

Figure 19: a 24-hour time series of Clear Days (CDs) and Fog Days (FDs) at Cattle Point (CP) plotted, with Air Temperature data from every 30 minutes. Data from summer 2021 – summer 2024 was used, based on available TRH data and time lapse camera images: 08/24/2021-09/30/2021, 07/21/2022-09/30/2022, 07/16/2023- 09/30/2023, and 07/15/2024-09/30/2024. Each red line represents a CD, while a blue line represents an FD.

FD-temperature time series tend to be cooler than CDs, especially between 7:00 and 15:00pm. FDs and CDs are more similar in temperature later on in the afternoon and in the early morning.

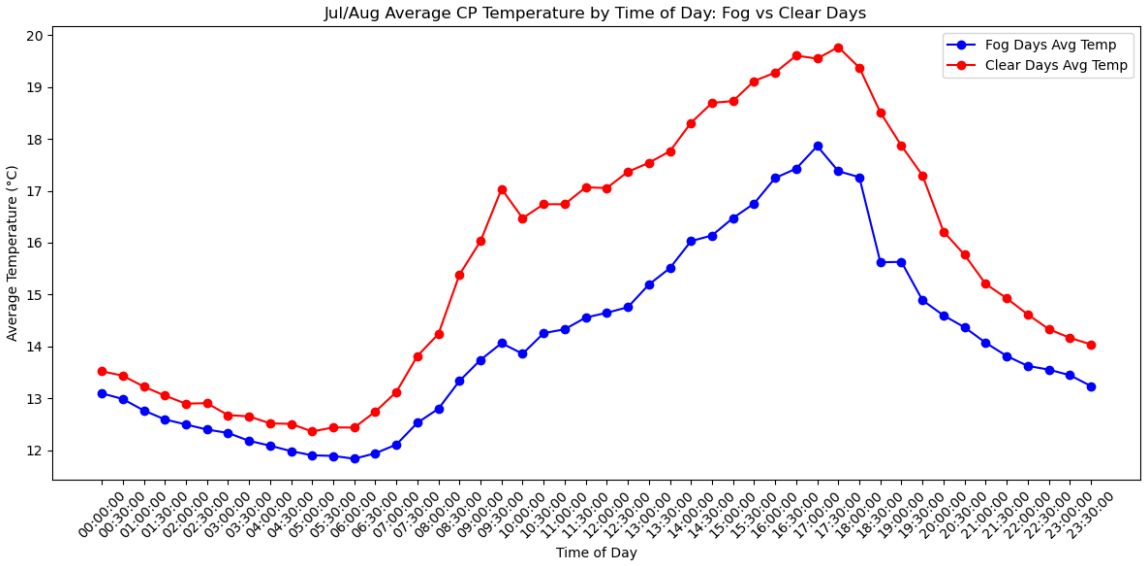

Figure 20: Average Air Temperature (°C) for FDs (blue) vs CDs (red) over a 24-hour time series at Cattle Point, with points every 30 minutes. The same data and date range was used as in Figure 19.

The mean temperature value every 30 minutes, calculated from the values in Figure 19, for FDs is lower than the mean value for CDs throughout the entire day. That difference gets larger at around 6:30am, stays pretty consistent until around 3:30pm, and then gets smaller again in the evening. There is a bump at the 9:00 – 9:30 mark in both lines that could be investigated more.

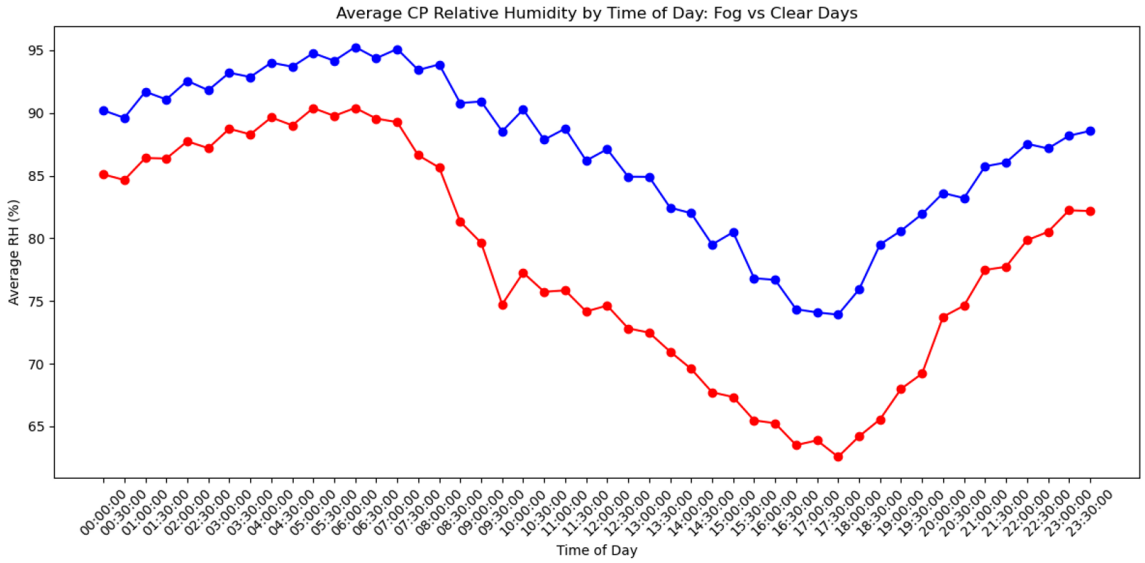

Figure 21: Average Relative Humidity (RH, %) for FDs (blue) vs CDs (red) at Cattle Point. The same data and date range was used as in Figure 19.

Average relative humidity for FDs is consistently higher that CDs throughout the 24-hour timespan (~95-74% vs ~89-62%, with the largest difference in value in the midday/early afternoon. A spike is visible in the CD plot at 9:00am, likely associated with the spike in Fig. 19.

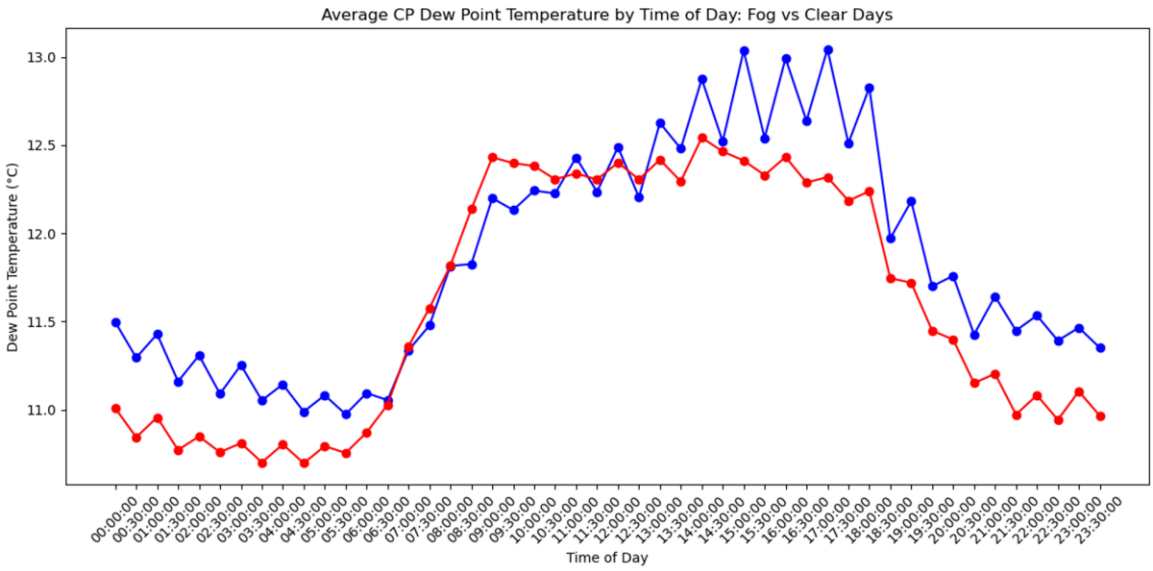

Figure 22: Average Dew Point Temperature (°C) for FDs (blue) vs CDs (red) at Cattle Point. The same data and date range was used as in Figure 19.

Average dew point temperature (DPT) values for FDs and CDs are closer in value over the 24-hour period. DPT for FDs is around 0.5°C higher than CDs in the morning, with values fluctuating up and down due to noise in the RH sensor, and the values match each other very well while increasing throughout the early morning. Late afternoons are also a time of interest, when FD values become larger again.

4.4 Ocean Profile Properties and CTD Cast Results

4.4.1 FHL Dock CTD Casts – July 9, 2025

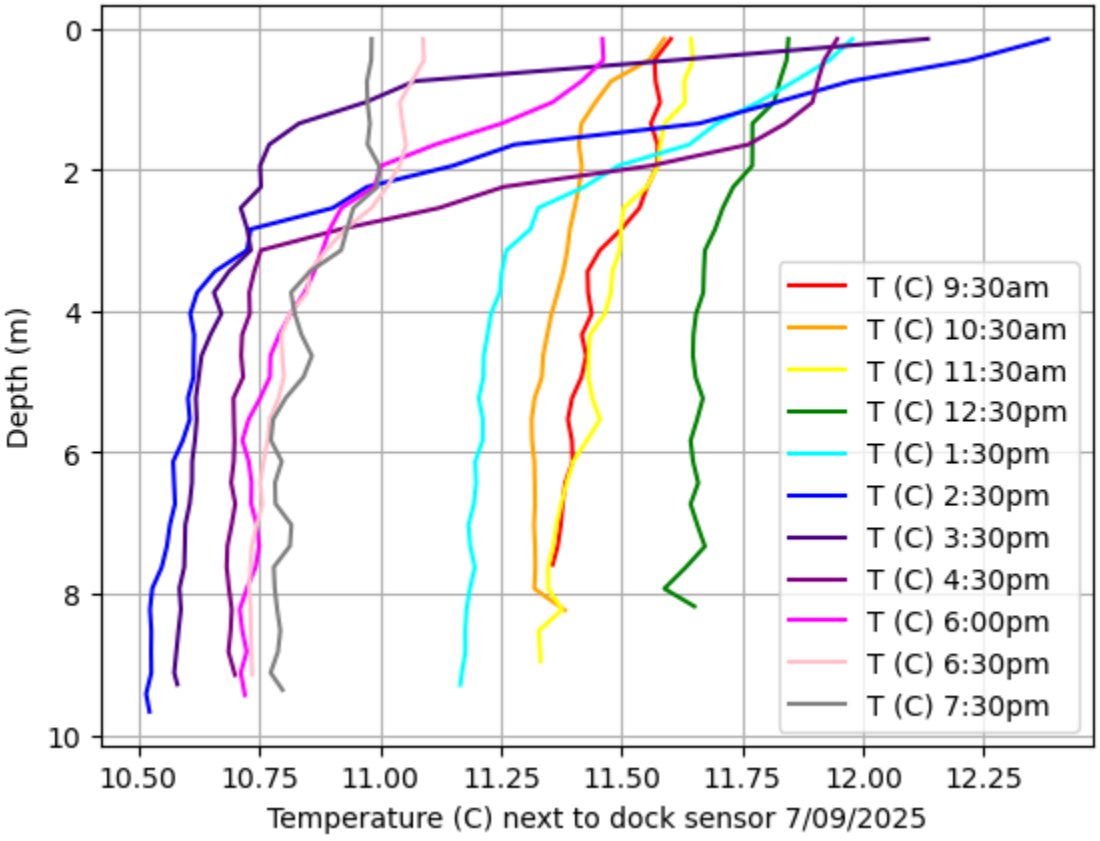

Figure 23: 2025-07-09 CTD profiles of Temperature (°C) off the FHL dock, taken every hour from 9:30am to 7:30pm. Low tide was at 10:35am, and high tide was at 7:40pm.

Early CTD casts (9:30am – 11:30am) look very uniform from top to bottom, with values ranging between 11.3°C near the bottom and 11.6°C at the surface. As the tide reaches its fastest rate of increasing water level, the water temperature profile becomes much more stratified, with the top layer remaining the warmest (and even becoming a little warmer, as we see with the 2:30pm and 3:30pm casts), and the deeper water becoming much colder. As that rate begins to decrease again, like in the 4:30pm and 5:30pm casts, the top layer of water begins to cool to match the temperature of the deeper water, before the profile becomes almost uniform again at 7:30pm, now at colder values between 10.75-11°C.

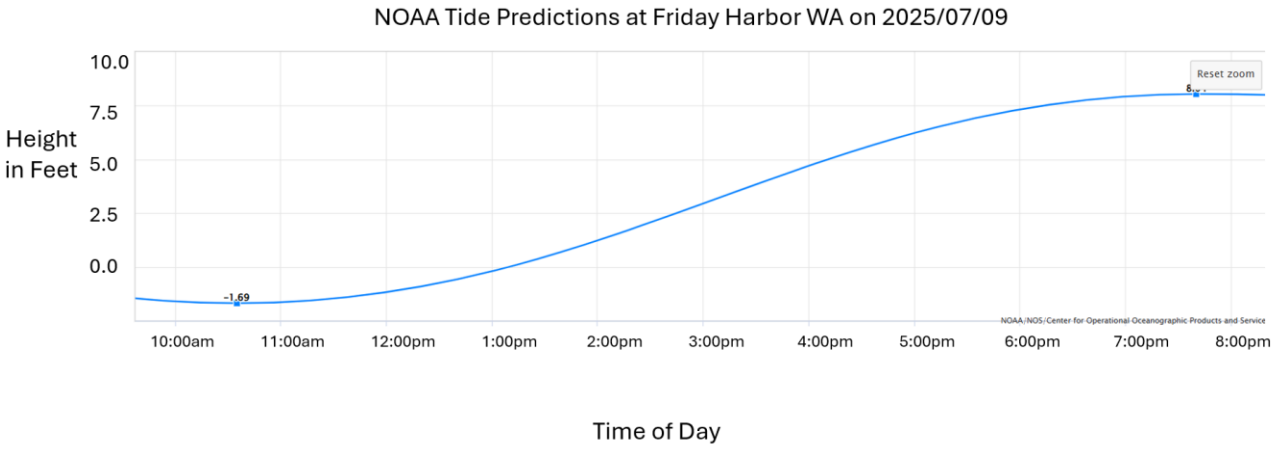

Figure 24: Tide predictions taken from the NOAA website for 2025-07-09 from 10:00am to 8:00pm

https://tidesandcurrents.noaa.gov/noaatidepredictions.html?id=9449880&units=standard&bdate=20250709&edate=20250709&timezone=LST/LDT&clock=12hour&datum=MLLW&interval=hilo&action=dailychart

4.4.2 Field Excursion CTD Casts

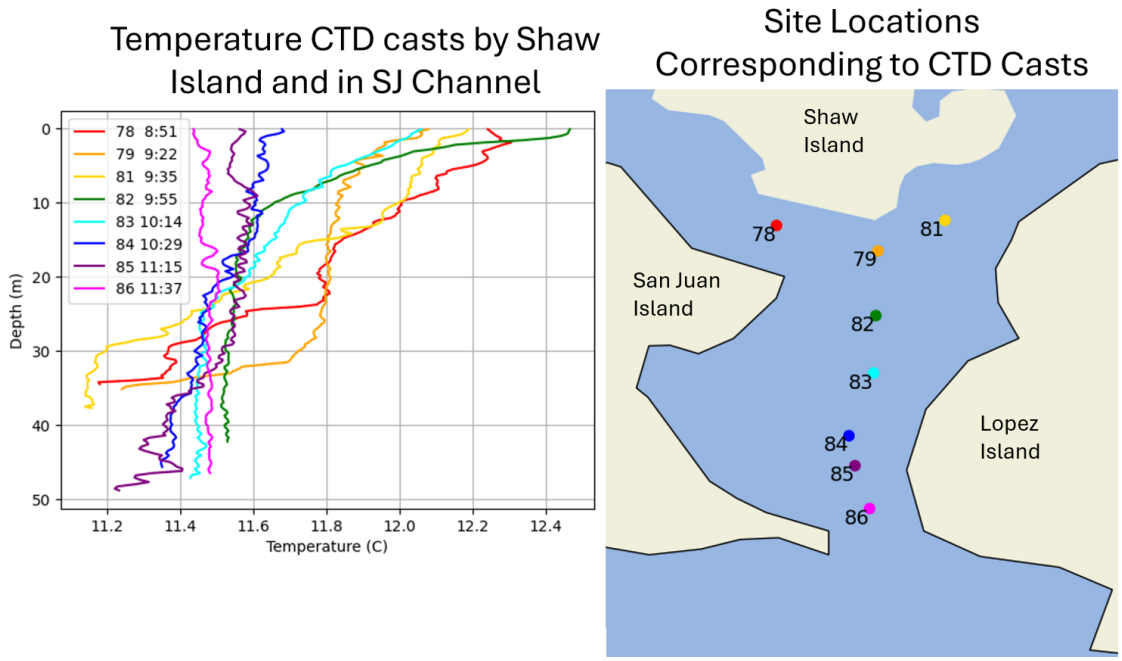

Figure 25: Left: CTD casts showing temperature vs depth, along with locations. Color of temperature profile corresponds to the color of the dot in the right map. Right: a map of the San Juan Channel, with each dot representing a coordinate location of a CTD cast. The arrow shows the direction of the tide as these casts were made.

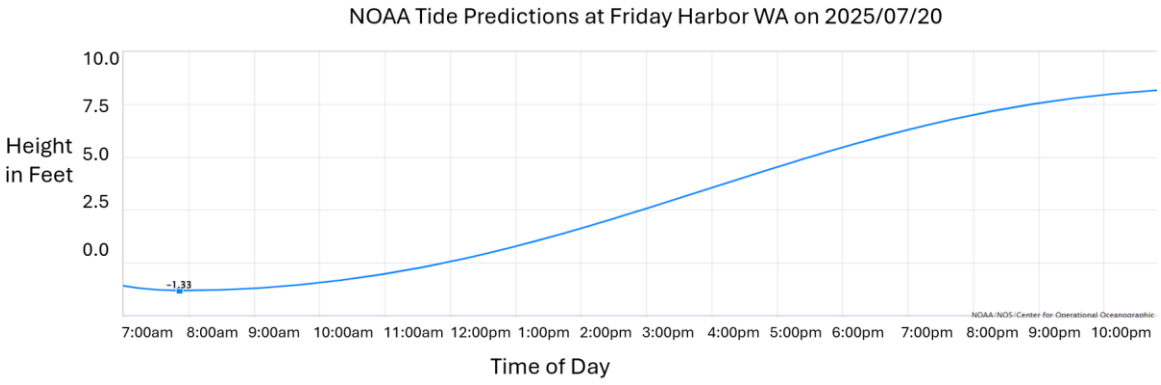

Figure 26: Tide predictions taken from the NOAA website for 2025-07-20 from 7:00am to 10:00pm.

https://tidesandcurrents.noaa.gov/noaatidepredictions.html?id=9449880&units=standard&bdate=20250709&edate=20250709&timezone=LST/LDT&clock=12hour&datum=MLLW&interval=hilo&action=dailychart

The first three casts, taken across the south end of Shaw Island, are the most stratified in temperature, ranging from values near 12.2° at the surface and around 11.2°C at around 35 meters. As we moved south through the channel, the temperature profile became much more uniform from top to bottom, with values from the last cast at 11:37am ranging between 11.4°C and 11.5°C. Casts from the middle of our trajectory, 82 and 83, looked similar to later casts at depth, starting at around 20m, but still were somewhat stratified in the top layer of water.

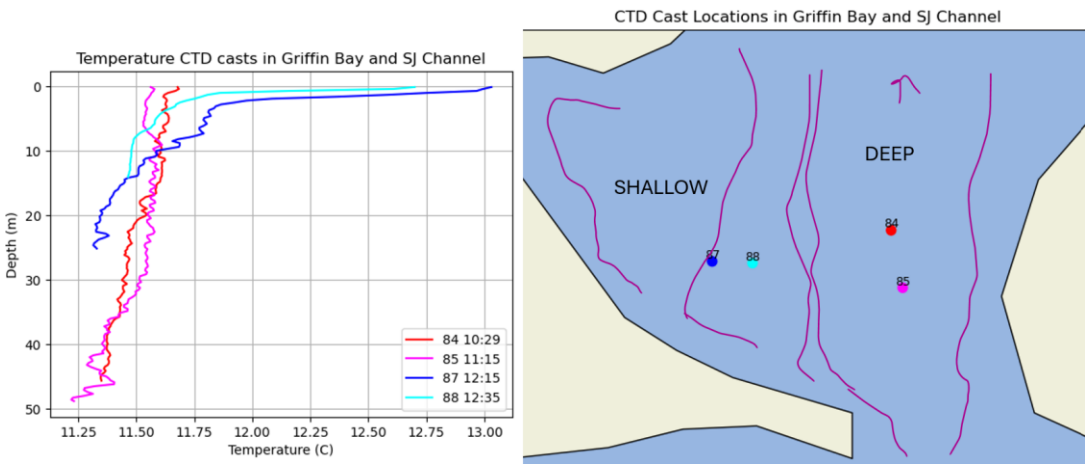

Figure 27: Left: CTD casts showing temperature vs depth, taken in Griffin Bay and the San Juan channel. Right: A map of the San Juan Channel and Griffin Bay, with lines representing rough bathymetry.

Casts from out in the open channel, 84 and 85, are very uniform from top to bottom (~45m), with a slight decrease in temperature further down. In comparison, casts take in Griffin Bay were extremely stratified, with recorded values ranging from around 13°C to 11.3°C and most of that temperature change occuring in the top 10 meters of the water column. Notable current speed differences were recorded; in the open channel near Cattle Point, drift speeds of 3.5-4 knots were reported by the boat's navigation software, while in the south end of Griffin Bay, the drift speed was reported to be 0.6 knots.

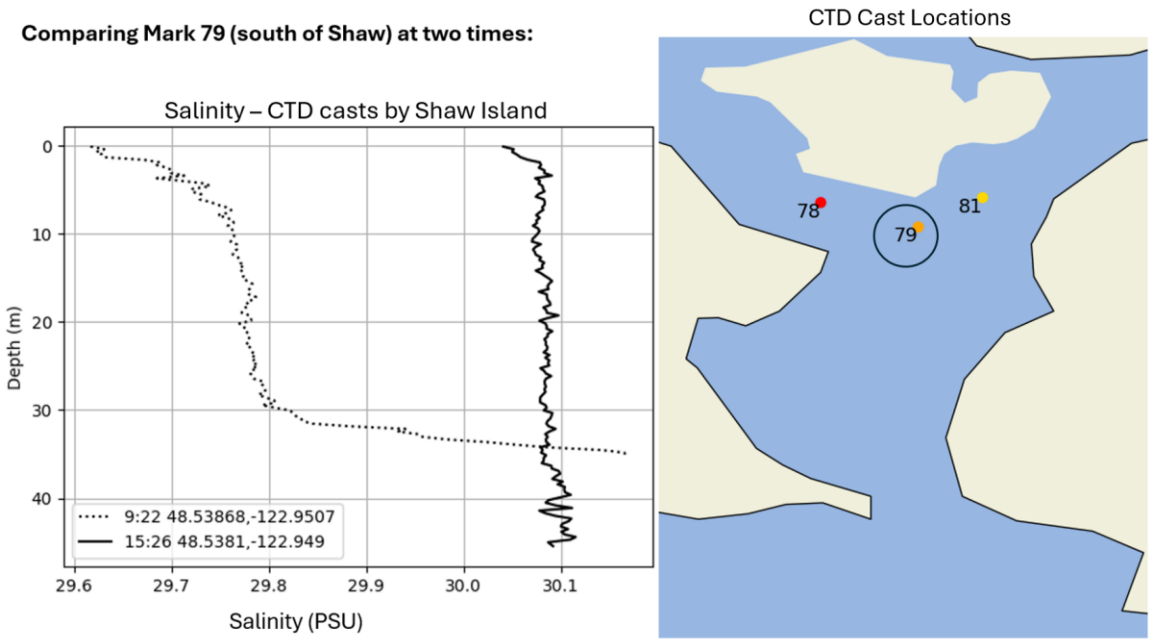

Figure 28: Left: two CTD profiles of salinity (PSU) done at mark 79, 6 hours apart. The dotted line is in the morning at 9:22am, near the beginning of the rising ride, while the solid line is at 3:25pm, further into the tidal cycle.

The 9:22am profile is much more stratified than the 3:26pm profile, with salinity values between 29.6 and 30.2, compared to values between 30.04 and 30.12 for the later

cast. Additionally, the 3:26pm cast is much saltier overall than the 9:22am cast, especially in the top 30 meters of the water column.

5. Discussion

5.1 SST vs AT Differences

From our plots of SST vs AT difference, we can see that positive SST differences tend to correspond to positive AT difference. However, we don't have enough data to further describe their relationship. It is still unclear whether a larger difference in SST between two locations results in a larger difference in air temperature. Variation in difference values points us to look at the effects of other atmospheric processes. The unclear relationship between SST and AT could be due to other factors such as wind speed and direction, cloud cover/solar exposure, tidal patterns and currents, and urban heating. Accounting for these factors and collecting more data may reveal a clearer connection between temperature differences in the future. Additionally, developing a more consistent and frequent method of collecting SST data would be very helpful for comparing SSTs and ATs across different locations.

5.2 Mean Landsat Image

When we look at a map of the bathymetry and depth of the water around San Juan island, we can see that the patches of colder water mentioned in Section 4.2 seem to exist over areas with deeper water, and align along steep inclines where the water goes from being very deep to very shallow over a small stretch of distance. For example, in the San Juan Channel, water out in the open channel is deeper than in Griffin Bay. Based on this information, we believe that the patches of colder surface water that we see with Landsat are at least partially due to mechanical mixing effects from the local geography of the region. This could explain some of the differences in SST between the north and south

ends of the island; not only does warm water have to make it all the way down the San Juan Channel to reach Cattle Point, but there also appears to be additional upwelling there that would cool the surface water. This is discussed more in section 5.4.

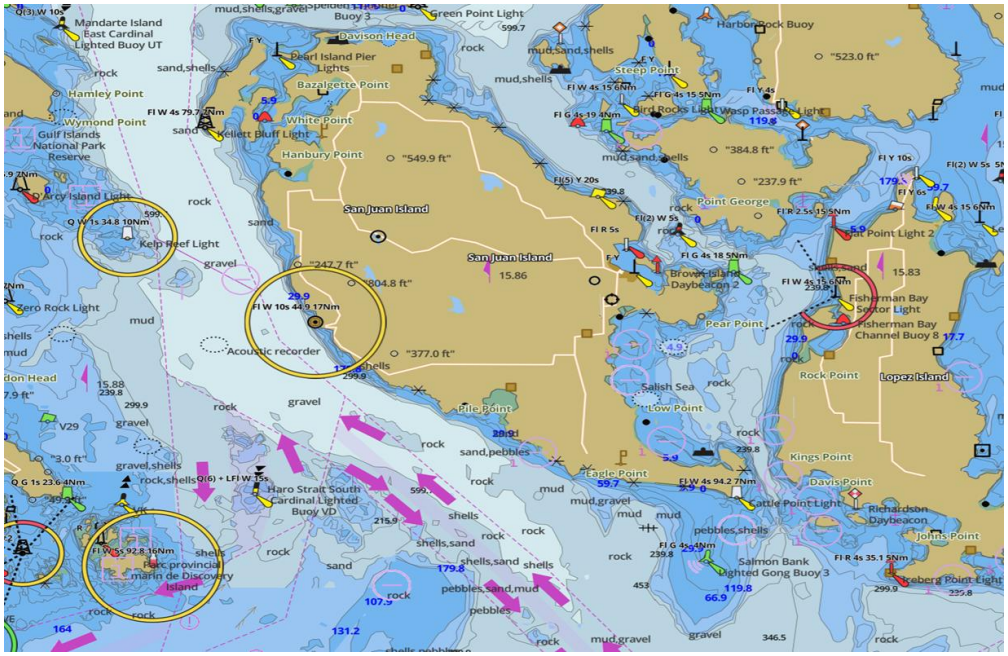

Figure 29: Bathymetry map around San Juan Island from https://fishing-app.gpsnauticalcharts.com/i-boating-fishing-web-app/fishing-marine-charts-navigation.html?title=SAN+JUAN+CHANNEL+boating+app#12/48.5250/-122.9900. Darker blue represents shallower water; lighter blue represents deeper water. Other markings like yellow circles and pink arrows should be ignored; only water color (depth) is relevant.

More Landsat scenes could be used to contribute to the stacked image if we developed a cloud mask, which would allow us to average only pixels representing water temperatures. Our presented stacked Landsat image is only based on scenes from 8 days, all at noon. It is useful in looking at SST patterns qualitatively, especially when compared

to current models and geography. However, it doesn't account for differences in points in the tidal cycle and water circulation that could affect the ocean surface in different ways across different days.

5.3 Fog vs Air Temperature

From our time series, we can see that FDs tend to be on the cooler end of the air temperature spectrum, and on average, throughout the entire day, they are cooler than CDs. Additionally, we can see that especially in the morning, they have a higher Dew Point Temperature and higher relative humidity than CDs. These patterns are consistent with our definitions and current knowledge about the conditions that coastal fog forms and dissipates under. Further analysis of these days and air temperature may help us get a better idea about the specific range of temperature, RH values, and DPTs that matter for this phenomenon.

The bump in the temperature, DPT, and RH plots at the 9:00 – 9:30am mark is very likely due to days with odd temperature spikes in the morning, or sunlight directly hitting the sensor. From Figure 19, we can see that some FDs had a spike in temperature around that time, 8:30am – 9:30am. Identifying which days experienced abnormal temperature and RH values and looking into why they did could be useful. Better quantifying how much visibility is limited by fog and looking more at how long it persists across different days in relation to our TRH records would also be interesting. Additionally, days that had both fog and high cloud coverage were disregarded in this project but could be studied as well.

5.4 CTD casts

From the CTD casts off of the FHL dock, we can see that the water column is most stratified when the tide is rising the fastest – in the middle of the rising tide. Additionally, we can see that at the beginning of that cycle, when the tide is out, the water column is nearly uniform from top to bottom, and that by high tide, it is again almost uniform but sitting at a significantly different temperature. This information helped inform our knowledge of how tidal processes can affect stratification in a water column.

We used the CTD casts from the San Juan Channel to study the water column in different spots and compare them. First, the water closer to Cattle Pass is significantly more well-mixed than the water to the North in the early part of a tidal cycle. This was especially interesting because we might have expected that there would be at least some stratification in the temperature profile, as cold water gets brought northward further down in the water column. That temperature profile differed from the smaller-scale profile of the water by the FHL dock, which remained stratified to an extent almost until the tide peaked. The uniform water profile at Cattle Pass could be due to mechanical mixing caused by local topography, as discussed in section 5.2. Visually, while at Cattle Pass, we observed very fast currents and abnormal current patterns, including small whirlpools and eddies. With the IR temperature sensor, we measured varying water temperatures ranging 9-12°C over very short distances and periods of time. A more in-depth CTD study in Cattle Pass over a longer course of time would tell us more about how the water column structure changes through the tidal cycle.

Second, the water in Griffin Bay is significantly more stratified than the water in the open channel. This could be due to its removal from the direct path of strong currents, and its shallower depth. If there is less mixing happening in the bay, the water is more

able to be heated by the sun and develop more distinct layers. Figure 27 shows how much the water profile can vary over a relatively small horizontal distance.

Third, the profile of an individual location can change dramatically over the course of several hours, as we see with mark 79. Additionally, we can see how much density and salinity can vary in the water column, very deep in the water. The salinity profile depicted in Figure 28 shows a dramatic increase in salinity of the water at about 30 meters down, giving us a picture of how the tide was bringing saltier water. Our cast might not have fully captured the extent to which salinity was changing at depth, as we didn't take CTD measurements any deeper than around 40 meters.

5.5. Future Work

There are many directions to go with this work in the future. Gathering wind speed and direction data, as well as expanding our TRH sensors and time lapse cameras to more locations (and even other islands), would allow us to gather larger local datasets and understand more of the small-scale processes affecting conditions around the island. Our study this year primarily focused on the east side of San Juan Island – the west side is still a possibility to be explored.

We used a small dataset this summer that we could expand by using data from more satellites in the future. As this project continues, we will add onto our TRH and time-lapse camera records and gain more information to use those images to with, to compare SSTs, air temperature, and other air properties.

A past study done by FHL students in 1999 looked at three places in the San Juan Channel in detail and some interesting patterns about how the water circulates there

(Banas et al., 1999). A more in-depth field campaign, using a boat and CTD, to measure water properties at key locations over longer periods of time, would be very informative regarding how water circulation around San Juan Island functions, and would explain more about the surface temperature differences we have observed so far.

6. Acknowledgements

This research was supported by NSF Grant DBI-2149705.

We would like to express our immense gratitude to the FHL REU coordinators for all of the hard work they put into the program this summer and the support they provided. Additionally, thank you to all the San Juan Island community members for allowing us to deploy field equipment on your property – Megan and David, George and Peggy, Susan and Ana Mari, Diana, Scott, and Jim.

Thank you to Eli Schwat for all of your technical support and flexibility to hop on Zoom and even come up to the island for a few days. Thank you to Emily Carrington, for access to the FHL weather station data, and thank you to Parker MacCready, for all of the high-resolution LiveOcean model data.

Bibliography

Banas, N., Bricker, J., Carter, G., Gerdes, F., Martin, W., Nelson, E., Ross, T., Scansen, B., Simons, R., & Wells, M. (1999, September 1). *Flow, stratification, and mixing in San Juan Channel: Coastal and estuarine geophysical fluid dynamics Oc590b* (Student report). Friday Harbor Laboratories, University of Washington. https://www.ocean.washington.edu/research/gfd/FHL99-student-report-SanJuanChannel.pdf

Bashevkin, S., Lee, D., Driver, P., Carrington, E., & George, S. (2016). Prior exposure to low salinity affects the vertical distribution of Pisaster ochraceus (Echinodermata: Asteroidea) larvae in haloclines. *Marine Ecology Progress Series*, *542*, 123–140. https://doi.org/10.3354/meps11563

Borgnino, M., Desbiolles, F., Meroni, A. N., & Pasquero, C. (2025). Lower Tropospheric Response to Local Sea Surface Temperature Anomalies: A Numerical Study in the EUREC4A Region. *Geophysical Research Letters*, *52*(1). https://doi.org/10.1029/2024gl112294

Dye, A., Rauschenbach, S., De Szoeke, S., Igel, A. L., Jin, Y., Kim, J. B., Krawchuk, M. A., Maes, K., O'Neill, L., Paw U, K. T., Samelson, R., Shaw, D. C., & Still, C. (2024). Fog in western coastal ecosystems: Inter-disciplinary challenges and opportunities with example concepts from the Pacific Northwest, USA. *Frontiers in Environmental Science*, *12*. https://doi.org/10.3389/fenvs.2024.1488401

Earth Resources Observation and Science (EROS) Center. (2017). *Landsat 8 Operational Land Imager / Thermal Infrared Sensor Level-1, Collection 1* [Tiff]. U.S. Geological Survey. https://doi.org/10.5066/F71835S6

Feld, S. I., Cristea, N. C., & Lundquist, J. D. (2013). Representing atmospheric moisture content along mountain slopes: Examination using distributed sensors in the Sierra Nevada, California. *Water Resources Research*, *49*(7), 4424–4441. https://doi.org/10.1002/wrcr.20318

Fernando, H. J. S., Dorman, C., Pardyjak, E., Shen, L., Wang, Q., Creegan, E., Gaberšek, S., Gultepe, I., Hoch, S., Lenain, L., Richter, D., Chang, R., VandenBoer, T. C., Bardoel, S., Barve, A., Blomquist, B., Bullock, T., Chen, Z., Colosi, L., … Yamaguchi, R. (2025). Fatima-GB: Searching Clarity within Marine Fog. *Bulletin of the American Meteorological Society*, *106*(6), E971–E1016. https://doi.org/10.1175/bams-d-23-0050.1

Helmuth, B., Harley, C. D. G., Halpin, P. M., O'Donnell, M., Hofmann, G. E., & Blanchette, C. A. (2002). Climate Change and Latitudinal Patterns of Intertidal Thermal Stress. *Science*, *298*(5595), 1015–1017. https://doi.org/10.1126/science.1076814

Jackson, J. M., Bianucci, L., Hannah, C. G., Carmack, E. C., & Barrette, J. (2021). Deep Waters in British Columbia Mainland Fjords Show Rapid Warming and Deoxygenation From 1951 to 2020. *Geophysical Research Letters*, *48*(3). https://doi.org/10.1029/2020gl091094

Jang, J.-C., & Park, K.-A. (2019). High-Resolution Sea Surface Temperature Retrieval from Landsat 8 OLI/TIRS Data at Coastal Regions. *Remote Sensing*, *11*(22), 2687. https://doi.org/10.3390/rs11222687

Johnstone, J. A., & Dawson, T. E. (2010). Climatic context and ecological implications of summer fog decline in the coast redwood region. *Proceedings of the National Academy of Sciences*, *107*(10), 4533–4538. https://doi.org/10.1073/pnas.0915062107

Khangaonkar, T., Nugraha, A., Xu, W., & Balaguru, K. (2019). Salish Sea Response to Global Climate Change, Sea Level Rise, and Future Nutrient Loads. *Journal of Geophysical Research: Oceans*, *124*(6), 3876–3904. https://doi.org/10.1029/2018jc014670

Koračin, D., Dorman, C. E., Lewis, J. M., Hudson, J. G., Wilcox, E. M., & Torregrosa, A. (2014). Marine fog: A review. *Atmospheric Research*, *143*, 142–175. https://doi.org/10.1016/j.atmosres.2013.12.012

Nguyen, A., Lundquist, J., Pestana, S., Schwat, E. (2023). Summer Fog Frequency Patterns and Impact on Intertidal Organisms around Washington Coast from GOES-17 Satellite Imagery, Field Photos, and Field Sensors. https://digital.lib.washington.edu/researchworks/items/fd8ed7f4-b2a2-4120-83c8-fcda25393200/full

MacCready, P., McCabe, R. M., Siedlecki, S. A., Lorenz, M., Giddings, S. N., Bos, J., Albertson, S., Banas, N. S., & Garnier, S. (2021). Estuarine Circulation, Mixing,

and Residence Times in the Salish Sea. *Journal of Geophysical Research: Oceans*, *126*(2), e2020JC016738. https://doi.org/10.1029/2020JC016738

MacCready, P., Xiong, J., Carini, R., & Newton, J. (2025). LiveOcean. *Benefits of Ocean Observing Catalog (BOOC)*, *3*(1). https://doi.org/10.15351/3068-2320.1117

Mass, C., Randall, C., Conrick, R., & Ovens, D. (2022). The Relationship between Northeast Pacific Sea Surface Temperatures, Synoptic Evolution, and Surface Air Temperatures over the Pacific Northwest. *Weather and Forecasting*, *37*(10), 1741–1759. https://doi.org/10.1175/waf-d-22-0069.1

Miller, S. T. K., Keim, B. D., Talbot, R. W., & Mao, H. (2003). Sea breeze: Structure, forecasting, and impacts. *Reviews of Geophysics*, *41*(3), 2003RG000124. https://doi.org/10.1029/2003RG000124

Mislan, K. A. S., Wethey, D. S., & Helmuth, B. (2009). When to worry about the weather: Role of tidal cycle in determining patterns of risk in intertidal ecosystems. *Global Change Biology*, *15*(12), 3056–3065. https://doi.org/10.1111/j.1365-2486.2009.01936.x

Mizuta, D. D., Kasai A., Ken-Ichiro I., Yamaguchi H., & Nakata H. (2014). Effects of artificial upwelling on the environment and reared oyster *Crassostrea gigas* in Omura Bay, Japan. Bull. Japan. Soc. Sci. Fish, 78 (1) 13–27. https://www.researchgate.net/profile/Darien_Mizuta/publication/271193405_Effects_of_artificial_upwelling_on_the_environment_and_reared_oyster_Crassostrea_gigas_in_Omura_Bay_Japan/links/5644a81b08ae9f9c13e56557/Effects-of-

artificial-upwelling-on-the-environment-and-reared-oyster-Crassostrea-gigas-in-Omura-Bay-Japan.pdf?origin=scientificContributions

O'Brien, T. A., Sloan, L. C., Chuang, P. Y., Faloona, I. C., & Johnstone, J. A. (2013). Multidecadal simulation of coastal fog with a regional climate model. *Climate Dynamics*, *40*(11–12), 2801–2812. https://doi.org/10.1007/s00382-012-1486-x

Pawlowicz, R., Hannah, C., & Rosenberger, A. (2019). Lagrangian observations of estuarine residence times, dispersion, and trapping in the Salish Sea. *Estuarine, Coastal and Shelf Science*, *225*, 106246. https://doi.org/10.1016/j.ecss.2019.106246

Rastogi, B., Williams, A. P., Fischer, D. T., Iacobellis, S. F., McEachern, K., Carvalho, L., Jones, C., Baguskas, S. A., & Still, C. J. (2016). Spatial and Temporal Patterns of Cloud Cover and Fog Inundation in Coastal California: Ecological Implications. *Earth Interactions*, *20*(15), 1–19. https://doi.org/10.1175/ei-d-15-0033.1

Roemmich, D., & McGowan, J. (1995). Climatic Warming and the Decline of Zooplankton in the California Current. *Science*, *267*(5202), 1324–1326. https://doi.org/10.1126/science.267.5202.1324

Torregrosa, A., Combs, C., & Peters, J. (2016). GOES-derived fog and low cloud indices for coastal north and central California ecological analyses. *Earth and Space Science*, *3*(2), 46–67. https://doi.org/10.1002/2015ea000119

Vanhellemont, Q., Brewin, R. J. W., Bresnahan, P. J., & Cyronak, T. (2022). Validation of Landsat 8 high resolution Sea Surface Temperature using surfers. *Estuarine, Coastal and Shelf Science*, *265*, 107650. https://doi.org/10.1016/j.ecss.2021.107650

Wachmann, A., Starko, S., Neufeld, C. J., & Costa, M. (2024). Validating Landsat Analysis Ready Data for Nearshore Sea Surface Temperature Monitoring in the Northeast Pacific. *Remote Sensing*, *16*(5), 920. https://doi.org/10.3390/rs16050920